Miodrag D. Milenković-Babić
Section Head
Computational aerodynamics and control
Military Technical Institute (VTI) Belgrade

Branislav G. Ostojić
Research Engineer
Military Technical Institute (VTI) Belgrade

Nemanja Z. Ristić
Research Engineer
Military Technical Institute (VTI) Belgrade

Biljana Z. Dovatov
Head of Aerodynamic Department
Military Technical Institute (VTI) Belgrade

Vuk D. Antonić
Lead Research Engineer
Military Technical Institute (VTI) Belgrade

Dijana B. Damljanović
Section Head
Experimental Aerodynamics Laboratory
Military Technical Institute (VTI) Belgrade

Boško P. Rašuo
Full-Professor
University of Belgrade
Faculty of Mechanical Engineering

Compensation of Motor Torque Asymmetry During the Take-off Phase of an X-tail Unmanned Aerial Vehicle

The use of Unmanned Aerial Systems is expanding rapidly across civil and military domains, with sustained growth anticipated in the coming decades. The X-tail UAV configuration, characterized by the absence of ailerons and higher wing loading, offers excellent maneuverability for loitering munition applications. However, the design requires extreme control derivatives to maintain flight quality, and the minimal air-speed is determined by both lift capability and the ability to counteract propulsion torque. This research systematically examines the latter factor. Brushless direct current motor was first characterized experimentally, followed by testing with five propeller types to evaluate maximum revolutions per minute and power input. Among the tested configurations, the 18×11-inch propeller achieved 6,390 revolutions per minute at peak power, demonstrating the most favorable trade-off between thrust and torque. Wind tunnel tests at zero airspeed and simulated take-off velocity validated the integrated propulsion performance, showing excellent agreements with the theoretical predictions. The results confirm the suitability of the chosen motor–propeller combination and establish a minimum launcher-assisted take-off speeds as a function of altitude for defined UAV mass. These findings provide a robust basis for propulsion optimization in similar UAV configurations, supporting reliable and efficient operational deployment.

Keywords: *X-tail UAV; motor torque; wind tunnel measurement, propeller.*

1. INTRODUCTION

The Unmanned Aerial System (UAS) market value is growing every year, and a similar trend has been esti–mated for the next decades in Europe [1] and worldwide [2]. The expected annual growth rate is 14.91% in the next ten years according to the [2]. In this period many new UAVs will be designed and produced for military and civile application. All previous design [3-7] had different level of success on the market. Loitering munition systems have seen high demand in military applications [8–10]. These systems typically utilize a power-launch subsystem [11–13], since they are usually designed without landing gear and therefore require an external launch mechanism to initiate the take-off phase [12]. The most commonly used launchers are pneumatic and mechanical systems [13], due to their reliability and compact design. Pneumatic launchers, in particular, offer precise control of launch velocity and are suitable for field deployment under various conditions.

The X-tail configuration given in Figure 1, with wings that do not include ailerons [14], provides excellent manoeuvrability and allows for higher wing loading. The higher wing loading design approach enables greater initial acceleration during the take-off phase, but at the cost of reduced roll control authority compared to the classical aileron-on-wing design [15].

Figure 1. Functional model of the X-tail UAV

The first step in choosing a brushless direct current (BLDC) motor for a UAV is analysing the market [19–22] and previous experience. The UAV polar curve is previously defined with sufficient accuracy using stan–dard methods [23, 24], computational fluid dynamics (CFD) simulations [25], or wind tunnel tests. Usually, the information provided by the motor manufacturer includes: battery voltage, RPM/V (revolutions per mi–nute per volt), maximum efficiency, maximum current, dimensions, maximum power, and sometimes a recom–mended propeller and integrated propulsion charac–teristics [21]. Based on previous experience [26] and available motor on the market, the AXI 4130/20 GOLD LINE BLDC motor has been chosen due to its high reliability and similar power requirements. The motor tests were carried out using an AXI 4130/20 GOLD LINE brushless motor. It should be noted that a newer version, the AXI 4130/20 GOLD LINE V3, featuring minor performance improvements, is currently integ–rated in the UAV platform. Therefore, while the pre–sented results correspond to the earlier model, the latest version benefits from these enhancements. An adequate propeller for the X-tail UAV must be defined through a

Received: January 2026, Accepted: March 2026
Correspondence to: Dr Miodrag Milenković-Babić
Military Technical Institute, Ratka Resanovića 1,
11000 Belgrade, Serbia
E-mail: miodragmbm@yahoo.co.uk
doi: 10.5937/fme2602261M

systematic multidisciplinary analysis [27] based on the flight envelopes. In the first steps, the BLDC motor characteristics were experimentally measured [28, 29].

In order to choose an adequate propeller, or to first reduce the number of potential propellers at low Reynolds numbers, the data from [30, 31] should be used as a guide. Following the mention steps the five different propellers have been chosen for experimental testing. The motor input power and maximum RPM were measured in order to compare the propellers and find an adequate one.

The propulsion characteristics of the system integrated into the UAV were verified in the Experimental Aerodynamics Laboratory [32] of the Military Technical Institute (VTI) in Belgrade, [14]. The testing campaign was divided in two main stages. In the first stage, the propulsion characteristics were evaluated at zero airspeed in order to establish a baseline for static thrust and torque for different propeller configurations. In the second stage, the measurements were repeated at the estimated take-off speed to assess the influence of incoming airflow on propulsion performance. Excellent consistency between the measured results and the theoretical predictions was observed, confirming the accuracy of the applied aerodynamic and propulsion models. The agreement was especially evident after comparing the wind tunnel measured power and torque values for various propellers with the results obtained in previous experiments. These verified results, together with the estimated control derivatives, confirm the success of the UAV design and define the minimum power-launcher airspeed required to ensure a safe and reliable UAV take-off.

2. EXPERIMENTAL MEASUREMENTS

The powertrain of any UAV driven by a single electric motor usually consists of a battery as the main energy source, an electronic speed controller (ESC), a BLDC motor, and a propeller [18]. The battery supplies energy to the ESC, which typically converts the direct current (DC) from the battery into a three-phase trapezoidal supply through a six-switch bridge inverter. This inverter enables precise control of the motor's rotational speed using pulse width modulation (PWM) techniques, which modulate the three-phase signals by rapidly switching them on and off. Usually, the characteristics of the battery and ESC are considered constant, as they mainly depend on the manufacturing technology. Since all propellers will be tested under similar operating conditions, this assumption is sufficiently accurate for comparative analysis of different propellers. The mathematical model of the BLDC motor is thoroughly explained in [18] and will be repeated here. The characteristics of the AXI 4130/20 GOLD LINE BLDC motors are given in Table 1.

The selected power source is an 8S LiPo battery configuration, consisting of eight cells connected in series. Given a nominal voltage of 3.7 V per cell, the total nominal pack voltage is 29.6 V. For accurate characterization of the motor's performance, tests should be conducted within a supply voltage range of 25–30 V, representing typical operating conditions corresponding to partial battery discharge. The obtained results are presented in the next section.

Table 1. Technical specifications of the AXI 4130/20 BLDC motor

Technical specifications	Gold Line	Gold Line V3
Number of cells	6-8s Li-Poly	6-8s Li-Poly
RPM/V	305 RPM/V	305 RPM/V
Maximal efficiency	88%	90%
Maximal efficiency current	18-40 A (>84%)	18-40 A (>84%)
No load current	1.2 A	1.1 A
Current capacity	55 A/60 s	56 A/60 s
Internal resistance	99 mΩ	43 mΩ
Dimension (diameter × length)	49.8 × 65.5 mm	49.8 × 64.4 mm
Shaft diameter	6 mm	6 mm
Weight	0.409 kg	0.410 kg

As described in [18], a dedicated motor test bench concept was employed for parameter identification. In the present work, this setup was implemented using the following measurement equipment:

- Current measurement: a precision 1 mΩ shunt resistor to monitor the current drawn from the power supply.
- Rotational speed measurement: an incremental encoder with 60 pulses per revolution mounted on the motor test bench, providing adequate resolution for speed determination.
- Torque measurement: a load cell (CCt Transducers 0.5–50 N range) mounted on a 50 mm torque arm connected to the braking system. The load cell output was conditioned using an HBM KWS3073 signal conditioner to ensure accurate and stable torque readings.

Additional devices used:

- Power supply: Aim-TTi CPX400DP, remotely controllable via GPIB–USB interface, enabling precise voltage and current control during testing.
- Data acquisition system: National Instruments USB-6211 DAQ module, used to acquire signals from all sensors and to transmit both the PWM motor control signal and the brake actuation signal to the test bench.

The measurement process was controlled by a custom-developed LabVIEW application, which allowed full customization of test parameters and ensured synchronized acquisition of all relevant measurement channels under the desired operating conditions.

The RPM measurements of five different propellers (Aeronaut CAM Folding: 16×10, 16×13, 17×11, 17×13, and 18×11 shown in Figure 2 from down to up) were conducted at the Laboratory for Experimental Modal Analysis, Vibration Analysis, and Balancing of the Aerospace Sector at the Military Technical Institute. During the tests, the following equipment was used: Brüel & Kjær (B&K) LAN-XI 3053-B-12/0 data acquisition system, MM 0360-100142 tachometer probe, and BK Connect 2021 software for data processing. The measurement equipment used in the tests is illustrated in Figure 3.

The battery intended for use on the UAV was employed as the energy source, with the aim of obtaining results that closely replicate actual UAV

operating conditions. During the RPM testing, the voltage and current output from the ESC were monitored using ESC control software on a laptop. The averaged values are presented in the following section, along with the measured motor RPM.

Figure 2. Experimental tested propellers

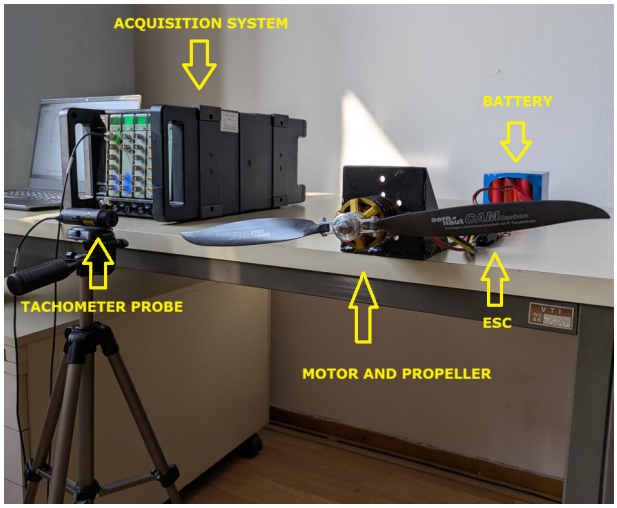

Figure 3. Experimental measurement equipment

Wind tunnel testing of the full-scale functional UAV model (FM) equipped with the integrated BLDC motor and propeller, as originally described in [14], was conducted at the T-35 subsonic wind tunnel facility of the Military Technical Institute (VTI) in Belgrade (see Figure 4).

This continuous-flow tunnel is powered by a 7.2 MW alternating current motor driving a 23-blade variable-pitch fan, capable of reaching Mach numbers up to 0.5. Adjustments to the Mach number are made by varying the fan's rotational speed and blade pitch. The tunnel achieves Reynolds numbers as high as 12×10^6 per meter, with total pressure in the test section reaching up to 120 kPa (1.2 bar), while static pressure remains atmospheric. Test durations are theoretically unlimited.

The wind tunnel features interchangeable octagonal test sections measuring 3.2 m by 4.4 m with solid walls. For the present series of tests, a section equipped with a vertical quadrant tail sting support was employed, allowing precise stepwise and continuous rotation of the model about all three axes (yaw, pitch, and roll).

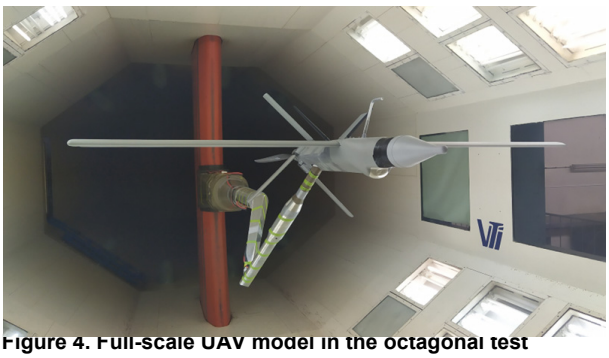

Figure 4. Full-scale UAV model in the octagonal test section of the VTI T-35 wind tunnel

Prior to and following facility upgrades, the flow quality of the VTI T-35 tunnel was thoroughly evaluated [33]. The Institute maintains rigorous periodic testing of standard models to ensure ongoing measurement reliability [34, 35].

To validate computational predictions, aerodynamic forces and moments on the flight model were measured using an Able Corporation Mk18 internal six-component strain gauge balance with a diameter of 50.8 mm. The Mk18 is a force balance assembly with an accuracy of approximately 0.2% full scale, accounting for hysteresis effects typical of its multi-component design.

3. RESULTS AND DISCUSION

Since the motor was tested within the voltage range corresponding to the selected 8S battery configuration (25–30 V), Figures 4 and 5 present the experimental data obtained under these supply conditions. As described in [18], a dedicated test bench was developed for motor parameter identification. The setup includes a remotely operated electromagnetic brake coupled with a force transducer for torque measurement. Motor rotational speed is recorded by an encoder, while a current shunt is used to measure the electrical current. Tests are performed at a fixed supply voltage and constant throttle (PWM), with the applied load adjusted via the brake.

The input power is determined as the product of the constant voltage and measured current. In rotational motion, the output power P is the product of torque Q and angular velocity ω. By measuring torque and RPM, and applying the relation:

$$\omega=\mathrm{RPM}\times2\pi/60, \tag{1}$$

it is possible to calculate the motor's output power and, subsequently, its efficiency. The motor efficiency is then obtained as the ratio of the output power to the input power. In these diagrams (Figure 4 and 5), the experimental measurements are represented by distinct markers, while the model results computed using parameters identified and averaged over all supply voltages are shown as coloured curves. Experimental results (Figures 4 and 5) show that, for currents between 18 and 40 A, the motor maintains an efficiency above 82%, with slightly higher efficiency observed at the 30 V supply voltage. Analysing the data presented in Figures 5 and 6, it is evident that with an increase in the nominal battery voltage, at the same power level, the motor torque decreases.

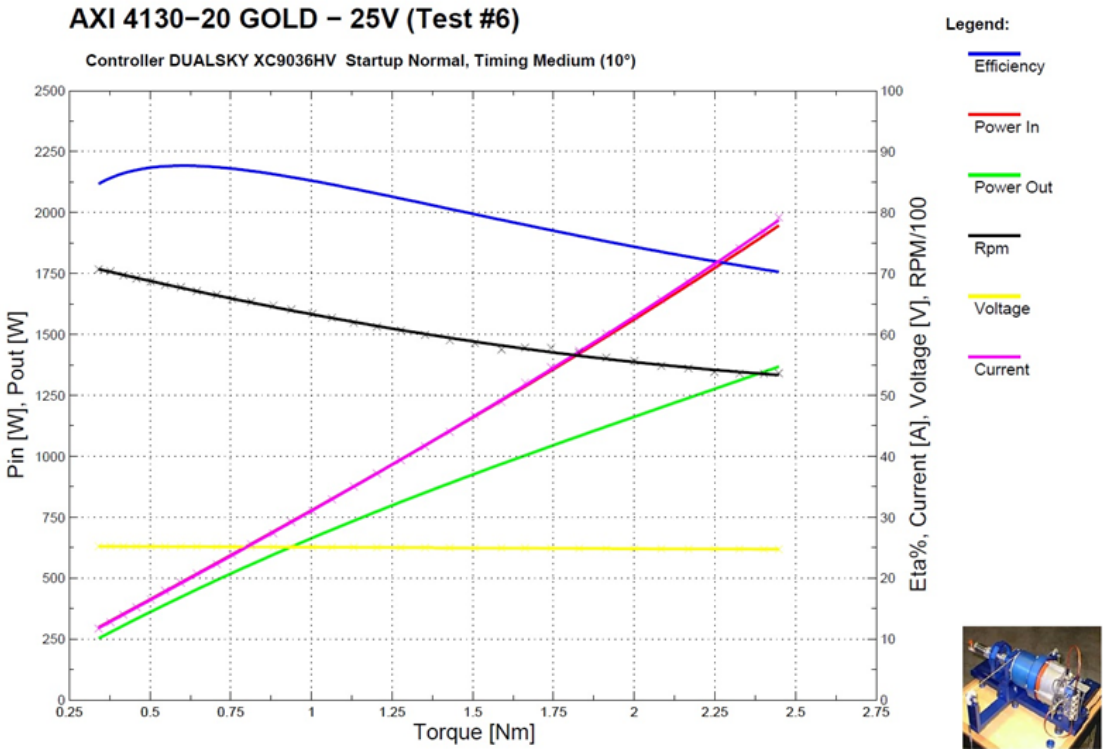

Figure 5. AXI 4130/20 GOLD LINE Motor test results at supply voltages of 25 V: Experimental measurements (markers) and identified model (solid lines)

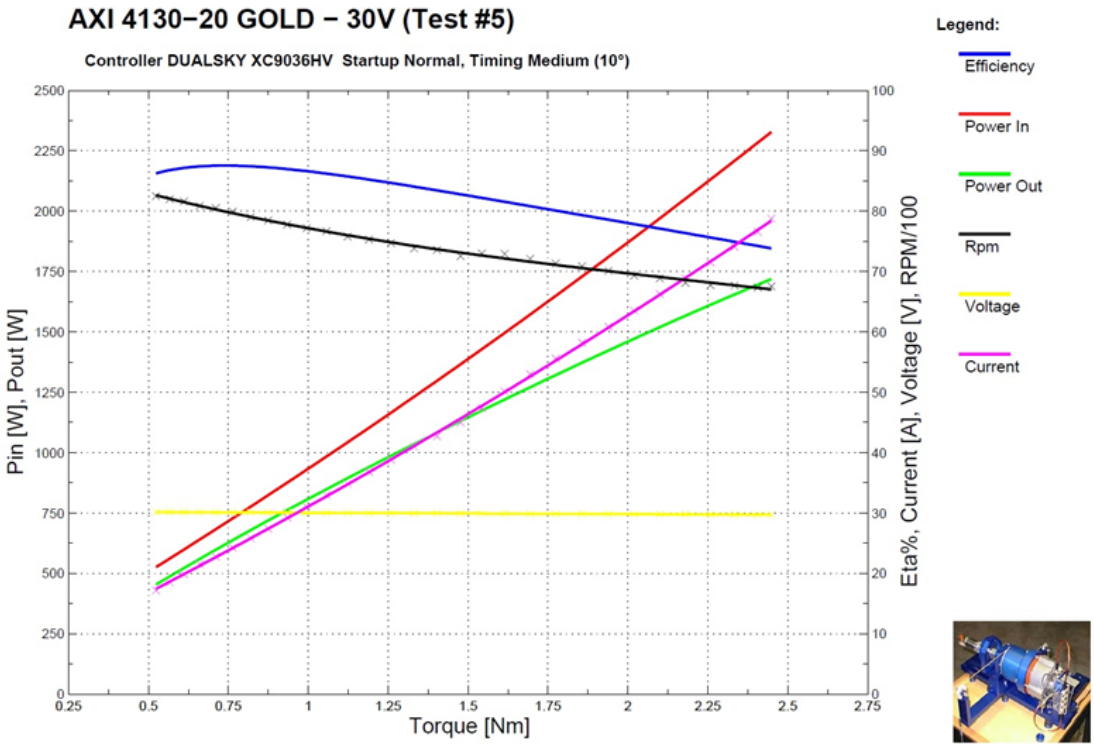

Figure 6. AXI 4130/20 GOLD LINE Motor test results at supply voltages of 30 V: Experimental measurements (markers) and identified model (solid lines)

In other words, the motor exhibits minimal torque at the maximum battery voltage, corresponding to the 8S configuration. It can be concluded that, in order to achieve the minimum motor torque, the maximum allowable nominal battery voltage is required, which in our case corresponds to the 8S battery configuration.

Table 2 presents the measured rotational speeds (RPM) for five Aeronaut CAM Folding propellers of different sizes: 16×10, 16×13, 17×11, 17×13, and 18×11. During these experiments, the output voltage and current from the ESC were continuously monitored using its control software running on a laptop computer. The input power values shown in Table 2 were calculated based on the averaged current and voltage measurements. Accordingly, Table 2 presents the propeller designations, their corresponding measured rotational speeds (RPM), and the calculated input power based on these averaged electrical values.

Table 2. Experimental results for propeller RPM and motor input power

Propeller	RPM	P [W]
16×10	6780	1276
16×13	6270	1400
17×11	6240	1404
17×13	5910	1458
18×11	6390	1456

Analysis of the data presented in Table 2, along with the identified motor parameters shown in Figures 5 and 6, indicates that the 16×10 propeller operates with over 10% lower power consumption compared to the other tested propellers. Consequently, this propeller was exc–luded from subsequent wind tunnel testing, since one of the UAV's goals is to achieve the highest acceleration during the take-off flight phase. Wind tunnel tests were conducted on the full-scale UAV model to measure the static performance of the propellers (torque and thrust force) for propellers sized 16×13, 17×11, 17×13, and 18×11 when integrated into the UAV. The obtained results are pre-sented in Table 3.

Table 3. The wind tunnel test results of measured torque and thrust force on propeller when it is integrated on UAV

Propeller	Thrust [N]	Torque [Nm]	T/Q [1/m]]
16×13	24	1.005	23.88
17×11	28.72	0.893	32.17
17×13	28.57	1.135	25.17
18×11	33	0.98	33.67

The data from Table 3 indicate that the 18×11 propeller has the highest static thrust force and the best force-to-torque ratio, making it the optimal choice for the take-off flight phase. A similar conclusion can be drawn from the data in Table 2, which show that the 18×11 propeller generates nearly the same power as the 17×13 propeller (1456 W compared to 1458 W), but at 8% higher RPM. The higher RPM corresponds to lower torque during the take-off phase. Based on this analysis, the 18×11 propeller was selected (see Figure 7) for the wind tunnel test corresponding to the take-off phase.

Figure 7 Aeronaut CAM Folding 18×11 propeller

It should be noted that the thrust force measured in the wind tunnel is reduced by the aerodynamic drag of the UAV components exposed to the propeller airflow. The same principle applies to the torque measurements. This explains why the measured thrust and torque values presented in Tables 3 are slightly lower than the expected values shown in Figures 5 and 6. On the other hand, the presented values represent the actual thrust force and torque that the propellers will deliver to the UAV when it is on the power-launcher at maximum throttle settings. This allows for the calculation of the maximum acceleration that the installed propulsion group can provide.

The minimal UAV airspeed and elevator control surface deflection, taken from [14], are approximately 14 m/s and –5.5°, respectively. The wind tunnel test data corresponding to the simulated take-off flight phase (estimated UAV airspeed of 14 m/s, corresponding to a Mach number of M = 0.04) are presented in Table 4. Table 4 shows the thrust results, representing the propeller thrust reduced by the UAV's drag at the specified airspeed. This reflects the actual force available to accelerate the UAV immediately after launch by the power launcher at the defined minimal airspeed, with the same principle applying to torque. The tests also make it possible to accurately determine the portion of the propulsion group's thrust available for acceleration in smaller UAVs that can be tested in wind tunnels, providing a precise assessment of post-launch acceleration performance. In practice, analytical calculations of these values are typically less precise and include a larger safety margin.

Table 4. Wind tunnel test results of the measured torque and thrust force of the 18×11 propeller integrated on the UAV at Mach number M = 0.04

Propeller	Thrust [N]	Torque [Nm]	T/Q [1/m]]
18×11	20.48	0.6	34.13

The rolling moment generated by the control surface is quite small compared to a typical aileron-on-wing configuration [14]. The minimal flight speed and propeller power optimization during take-off are defined based on lateral-directional maneuvering limitations [16, 17, 36]. The maximum control deflections for pitch, roll, and yaw motions must be estimated independently, and the sum of all three deflections in the worst case must be less than the available control deflection [14].

If the aerodynamics control surfaces deflection down is defined as positive (Figures 8), as it is expla–ined in [37], then the three apparent controls for pitch, roll, and yaw can be calculated by equations:

$$\begin{aligned} \delta_m &= \frac{1}{4}\left(\delta_1+\delta_2+\delta_3+\delta_4\right), \\ \delta_a &= \frac{1}{4}\left(-\delta_1-\delta_2+\delta_3+\delta_4\right), \\ \delta_r &= \frac{1}{4}\left(-\delta_1+\delta_2-\delta_3+\delta_4\right). \end{aligned} \tag{2}$$

The autopilot sends roll, pitch, and yaw commands to the actuators, which deflect the control surfaces as on a typical aircraft [37] or UAV configuration. Before they can be utilized, it is necessary to define the individual fin commands deflection as it is explained in [38]:

$$\begin{aligned} \delta_1 &= -\delta_a+\delta_m-\delta_r, \\ \delta_2 &= -\delta_a+\delta_m+\delta_r, \\ \delta_3 &= +\delta_a+\delta_m-\delta_r, \\ \delta_4 &= +\delta_a+\delta_m+\delta_r. \end{aligned} \tag{3}$$

It was shown that the necessary elevator deflection during the take-off phase is approximately –5.5°. With a typical maximum control surface deflection of 22-25°, the available aileron deflection is up to 11°.

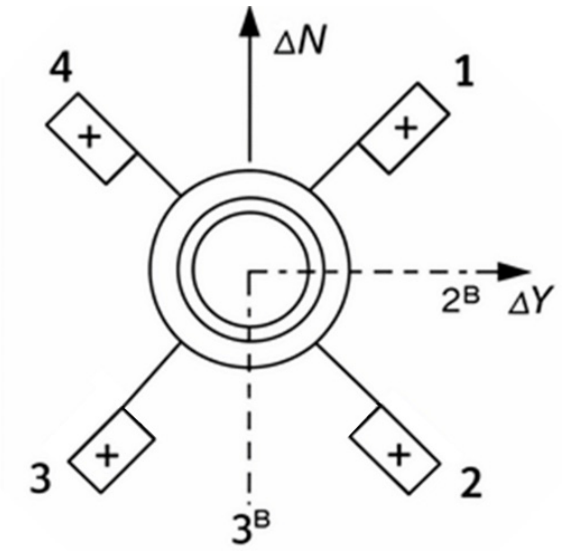

Figure 8. Definition of positive aerodynamic surface deflections (viewed from the rear)

Since the resultant deflection is the sum of the previous two, the aileron control power nonlinearity factor, K_A, must be included in the rolling moment equation (K_A=0.75). The maximum engine torque that can be compensated by the controls can be estimated using the following equation:

$$Q = 0.5 \cdot \rho \cdot V^2 \cdot S \cdot b \cdot C_{l\delta_a} \cdot \delta_{a-available} \cdot \mathrm{K}_A \cdot \qquad (4)$$

If the take-off is performed with the propeller operating while the UAV is still on the catapult, the torque values provided in Table 3 should be considered representative of this flight phase. It should be noted that the airflow around the UAV and propeller in the wind tunnel is primarily determined by the tunnel's capabilities rather than by the propeller itself, as would be the case in actual flight. Therefore, the values presented in Table 4 should be regarded as best estimation results.

In the presented configuration, the operation of the propeller increases the local Reynolds number in the X-tail region, which helps to delay or prevent airflow separation and consequently reduces the influence of the control power nonlinearity factor. This effect improves the overall roll control authority during the initial acceleration phase.

On the other hand, if the take-off is initiated without a running propeller, as is the case for certain UAV configurations [8, 9], the absence of this beneficial airflow modification can result in even greater torque values than those presented in Table 3, which must be taken into account when evaluating control surface effectiveness and ensuring adequate maneuvering margins.

In the worst-case scenario, assuming a take-off without the motor running, the required torque to be compensated is estimated at 1.6 Nm. With the rolling moment coefficient for aileron deflection estimated at 0.0917 1/rad from the wind tunnel test data given in [14], the minimal UAV airspeed that enables compensation of the engine torque is 17.06 m/s. At this speed, the calculated static torque that can be compensated is 1.601 Nm. As mentioned earlier, the take-off phase is not a static condition, and a safety margin should be included in the calculations. This is typically achieved either by increasing the minimum UAV airspeed by 10–15% or by accounting for the initial altitude by power-launcher and UAVs accele–ration capability.

4. CONCLUSION

The conducted experimental and analytical investiga–tions, including motor parameter identification, static thrust and torque measurements, and wind tunnel testing on a full-scale UAV model, have provided a compre–hensive assessment of propeller performance in various configurations. The results obtained from the motor-propeller characterization (Tables 1–4) clearly indicate that the selection of the optimal propeller for the take-off phase must consider not only the maximum thrust, but also the relationship between torque, rotational speed, and available control authority for lateral-directional manoeuvring.

The take-off configuration significantly affects both the aerodynamic environment around the control surfaces and the torque requirements to maintain lateral stability. A running propeller on the catapult not only increases the local Reynolds number in the X-tail region—delaying flow separation and mitigating control nonlinearity—but also ensures that the maximum expected engine torque remains within the values presented in Tables 3. Conversely, take-off without a running propeller can lead to higher torque loads and reduced roll control effectiveness, requiring careful consideration in control system design and flight safety assessments.

Based on comparative testing, the 18×11 propeller demonstrated the highest static thrust force and the most favourable thrust-to-torque ratio, making it the most suitable choice for the UAV's take-off requirements. The analysis further confirmed that the minimum safe take-off speed is approximately 17 m/s, which ensures sufficient aileron control authority to counteract engine torque. Additional safety margin of 10–15% is recommended to account for non-static conditions during the actual take-off phase.

Most importantly, the characteristics of the AXI 4130/20 BLDC motors have been determined for the voltage range corresponding to the selected 8S battery configuration (25–30 V), which is widely adopted. When combined with experimentally obtained propeller performance data, these results provide valuable insights for the aeronautical community. The presented design process is expected to play a key role in propulsion system sizing, control surface authority, and overall UAV performance during critical flight phases such as take-off.

ACKNOWLEDGEMENT

This study was supported by the Military Technical Institute (VTI), Belgrade. The authors would like to express their gratitude to Dr. Mario Silvagni from the Department of Mechanical and Aerospace Engineering – Mechatronics Laboratory, Politecnico di Torino, Italy,

for providing the experimental BLDC motor data and additional information on motor testing obtained through independent research.

FUNDING:

This research was funded by the Military Technical Institute (VTI) Belgrade and partly by the Ministry of Science, Technological Development and Innovation of Republic of Serbia (Project number 451–03–34/2026–03/200325).

REFERENCES

[1] Europe drone (UAV) market size. Available online: www.grandviewresearch.com/industry-analysis/europe-drone-uav-market-report

[2] Global unmanned aerial vehicles market overview. Available online: www.marketresearchfuture.com/reports/unmanned-aerial-vehicle-uav-market-806

[3] Janes, All the world's aircraft: unmanned, 2024–2025 yearbook.

[4] Saeed, A.S., Younes, A.B., Cai, C., Cai, G.: A survey of hybrid unmanned aerial vehicles, Progress in Aerospace Sciences, Vol. 98, 2018, pp. 91–105.

[5] Milenković-Babić, M., Ivković, D., Ostojić, B.: Flying wing conceptual design and flight testing, FME Transactions, Vol. 52, No. 4, 2024, pp. 556–562.

[6] Marin, M., Mirosavljević, P.: Analysis of the performance and kinematics of the movement of UAV, FME Transactions, Vol. 51, No. 4, 2023, pp. 627–636.

[7] Milenković-Babić, M., Stefanović-Goboljić, V., Ostojić, B.: The rescue system implementation in the medium range UAV, FME Transactions, Vol. 53, No. 3, 2025, pp. 482–489.

[8] Warmate loitering munitions system. Available online: www.wbgroup.pl/app/uploads/2017/06/warmate_eng_large_22q2.pdf

[9] HERO loitering munitions. Available online: https://uvisionuav.com/loitering-munitions/

[10] Jovičić, S., Jelisavac, J., Tomić, Lj., Obradović, I.: The effectiveness of the use of drones in modern conflict, 11th International Scientific Conference on Defensive Technologies – OTEH 2024, Tara, Serbia, October 2024, pp. 65–69.

[11] Khrulev, A.: Analysis of pneumatic catapult launch system parameters taking into account engine and UAV characteristics, Advanced UAV, Vol. 3, No. 1, 2023, pp. 10–24.

[12] Bek-Uzarov, M., Nenadić, I., Rašić, S.: Design and verification of a pneumatic launch system for a single-use UAV with a warhead, 11th International Scientific Conference on Defensive Technologies – OTEH 2024, Tara, Serbia, October 2024, pp. 60–64.

[13] Novaković, Z., Medar, N.: UAV launch systems, Armament Data – Fact Sheets, Military Technical Institute, Belgrade, Vol. XXXVIII, No. 156, 2015, ISBN 978-86-81123-76-8. (In Serbian)

[14] Milenković-Babić, M., Ostojić, B., Dovatov, B., Antonić, V., Nenadić, I., Damljanović, D.: Control derivative estimation of X-tail control surface design, Aerospace Science and Technology, Vol.163, August 2025. https://doi.org/10.1016/j.ast.2025.110343

[15] Smetana, F.: Computer assisted analysis of aircraft performance, stability and control, McGraw-Hill, New York, 1984.

[16] Stojaković, P., Rašuo, B.: Single propeller airplane minimal flight speed based upon the lateral mane–uver condition, Aerospace Science and Technology, Vol. 49, 2016, pp. 239–249. https://doi.org/10.1016/ j.ast.2015.12.012

[17] Stojaković, P., Velimirović, K., Rašuo, B.: Power optimization of a single propeller airplane take-off run on the basis of lateral maneuver limitations, Ae–rospace Science and Technology, Vol. 72, 2018, pp. 553–563. https://doi.org/10.1016/j.ast.2017.10.015

[18] Silvagni, M., Chiaberge, M., Tessari, F.: Analysis and modelling of powertrain components for an efficient UAV design, in: Ferraresi, C., Quaglia, G. (Eds.), Advances in Service and Industrial Robotics, RAAD 2017, Mechanisms and Machine Science, Vol. 49, Springer, Cham, 2018, pp. 503–515. https://doi.org/10.1007/978-3-319-61276-8_53

[19] AXI model motors. Available online: https://www.modelmotors.cz

[20] Plettenberg electrical motors. Available online: https://plettenbergmotors.com/products/electric-motors-en

[21] T-Motor – the safer propulsion system. Available online: https://store.tmotor.com

[22] Hacker brushless motors. Available online: https://www.hacker-motor-shop.com/brushless-motors.htm

[23] USAF stability and control DATCOM, McDonnell Douglas Corporation, Douglas Aircraft Division, 1978.

[24] Raymer, D.: Aircraft design: a conceptual approach, 5th ed., AIAA Education Series, 2012.

[25] Milenković-Babić, M., Dovatov, B., Ostojić, B., Antonić, V., Trifković, M., Ivković, D.: Tactical UAV flight performance estimation and validation, Defence Science Journal, Vol. 75, No. 1, January 2025,pp. 19–26. https://doi.org/10.14429/dsj.20276

[26] Antonić, V., Trifković, M., Molović, V., Milenković-Babić, M.: Small fixed-wing UAV pre–cision aerial drop capability development, Scientific Technical Review, Vol. 74, No. 2, 2024, pp. 65–70. https://doi.org/10.5937/OTEH24020 65A

[27] Abu Salem, A., Cipolla, V., Palaia, G., Binante, V., Zanetti, D.: A physics-based multidisciplinary app–roach for the preliminary design and performance analysis of a medium-range aircraft with box-wing architecture, Aerospace, Vol. 8, 2021, Article 292. https://doi.org/10.3390/aero space8100292

[28] Brezina, A., Thomas, S.: Measurement of static and dynamic performance characteristics of electric propulsion systems, 51st AIAA Aerospace Sciences Meeting including the New Horizons Forum and Aerospace Exposition, January 2013. https://doi.org/10.2514/6.2013-500

[29] Ghoddoussi, A.: A more comprehensive database for propeller performance validations at low Reynolds numbers, PhD Thesis, Wichita State University, 2016.

[30] APC propeller performance data. Available online: https://www.apcprop.com/technical-information/performance-data

[31] UIUC propeller data site. Available online: https://m-selig.ae.illinois.edu/props/propDB.html

[32] Damljanović, D., Vuković, Đ., Ocokoljić, G., Rašuo, B.: New transonic tests of HB-2 hypersonic standard models in the VTI T-38 trisonic wind tunnel, Aerospace, Vol. 12, 2025, Article 131. https://doi.org/10.3390/aerospace12020131

[33] Ocokoljić, G., Damljanović, D., Vuković, Đ., Rašuo, B.: Contemporary frame of measurement and assessment of wind-tunnel flow quality in a low-speed facility, FME Transactions, Vol. 46, 2018,pp.429–442. https://doi.org/10.5937/fmet1804429O

[34] Damljanović, D., Rašuo, B., Isaković, J.: T-38 wind tunnel data quality assurance based on testing of a standard model, Journal of Aircraft, Vol. 50, No. 4, 2013, pp. 1141–1149.

[35] Ocokoljić, G., Damljanović, D., Rašuo, B., Isaković, J.: Testing of a standard model in the VTI's large-subsonic wind-tunnel facility to estab–lish users' confidence, FME Transactions, Vol. 42, No. 3, 2014, pp. 212–218. https://doi.org/10.5937/fmet1403212O

[36] Nicolosi, F., De Marco, A., Sabetta, V., Della Vecchia, P.: Roll performance assessment of a light aircraft: flight simulations and flight tests, Aeros–pace Science and Technology, Vol. 76, 2018, pp. 471–483. https://doi.org/10.1016/j.ast.2018.01.041

[37] Milenković-Babić, M., Samardžić, M., Antonić, V., Marjanović, M. and Stefanović-Gobeljić, V.: Longitudinal stability characteristics of the LASTA airplane, Aircraft Engineering and Aerospace Technology, Vol. 89 Issue: 6, pp.911-919, 2018.

[38] Zipfel, P.: Modeling and simulation of aerospace vehicle dynamics, 2nd edition, AIAA education series, 2007.

NOMENCLATURE

UAS	Unmanned Aerial Systems
UAVs	Unmanned Aerial Vehicles
RPM	Revolutions Per Minute
BLDC	Brushless Direct Current
VTI	Military Technical Institute
CFD	Computational Fluid Dynamics
ESC	Electronic speed control
DC	Direct current
PWM	Pulse Width Modulation
FM	Functional model
B&K	Brüel & Kjær
P	Power [W]
T	Thrust [N]
Q	Torque [Nm]
ω	Angular velocity [rad/s]
ρ	Air density [kg/m^3]
V	Airspeed [m/s]
S	Area of the wing [m^2]
b	Wing span [m]
C_{lda}	Change in rolling moment coefficient with the aileron deflection [1/rad]
δ_a	Aileron control surface deflection [rad]
K_A	Aileron control power nonlinearity factor
δ_m	Elevator control surface deflection [rad]
δ_r	Rudder control surface deflection [rad]

КОМПЕНЗАЦИЈА МОМЕНТА МОТОРА У ФАЗИ ПОЛЕТАЊА БЕСПИЛОТНЕ ЛЕТЕЛИЦЕ СА УПРАВЉАЧКИМ ПОВРШИНАМА У КОНГИГУРАЦИЈИ Х-РЕПА

М. Миленковић-Бабић, Б. Остојић, Н. Ристић, Б. Доватов, В. Антонић, Д. Дамљановић, Б. Рашуо

Употреба беспилотних ваздухопловних система убрзано се шири у цивилним и војним доменима, при чему се у наредним деценијама очекује конти–нуирани раст. Конфигурација беспилотне летелице са Х-репом, коју карактерише одсуство крилаца и веће оптерећење крила, нуди изузетну управљивост за примене лутајуће муниције. Међутим, овај дизајн захтева екстремне управљачке деривативе како би се одржао задовољавајући квалитет лета, а минимална брзина лета одређена је како распо–ложивом силом узгона, тако и способношћу супрот–стављања обртном моменту погонске групе. Ово истраживање систематски разматра управо утицај погонске групе. Једносмерни електромотор без четикца најпре је експериментално окарактерисан, након чега су спроведена испитивања са пет различитих елиса ради процене максималног броја обртаја и улазне снаге. Међу тестираним конфигу–рацијама, елиса димензија 18×11 инча остварила је 6.390 обртаја у минути при максималној снази, показујући најповољније карактеристике између потиска и обртног момента. Испитивања у аеро–тунелу при нултој брзини струјања и при симу–лираној брзини полетања потврдила су интегрисане перформансе погонског система, уз одлично сла–гање са теоријским предвиђањима. Резултати потв–рђују оптималност изабране комбинације мотора и елисе и утврђују минималне брзине полетања уз помоћ лансера као функцију надморске висине за дефинисану масу беспилотне летелице. Спроведена анализа представљају поуздану основу за оптими–зацију погонске групе код сличних конфигурација беспилотних летелица.